Phenomenological characterization of photoactive centers in Bi12TiO20 crystals

Jaime Frejlich, Renata Montenegro, Nilson R. Inocente-Junior, Pedro V. dos Santos, Jean-Claude Launay, Christophe Longeaud, Jesiel F. Carvalho

Phenomenological characterization of photoactive centers in $Bi_{12}TiO_{20}$ crystals

Jaime Frejlich,[a] Renata Montenegro, Nilson R. Inocente-Junior, and Pedro V. dos Santos
Laboratório de Óptica, IFGW-UNICAMP, Campinas-SP, Sao Paulo 13083-970, Brazil

Jean Claude Launay
Institut de Chimie de la Matière Condensée de Bordeaux (ICMCB/CNRS), Université Bordeaux 1, 87 Avenue Dr. A. Schweitzer, 33608 Pessac, France

Christophe Longeaud
Laboratoire de Génie Electrique de Paris, UMR 8507 CNRS, Ecole Supérieure d'Electricité, Universités Paris VI et XI Plateau de Moulon, 91190 Gif-sur-Yvette, France

Jesiel F. Carvalho
Instituto de Física, Universidade Federal de Goiás, 94001-970, Goiânia-Go, Brazil

(Received 5 September 2006; accepted 5 December 2006; published online 16 February 2007)

We report optical and electrical measurements contributing for a better characterization of the relevant photoactive center levels in undoped photorefractive $Bi_{12}TiO_{20}$ (BTO) crystals grown in Brazil. Comparative results for Pb-doped BTO and $Bi_{12}GaO_{20}$ are also reported. A center responsible for photochromism was identified at 0.42–0.44 eV, probably below the conduction band (CB). The main electron and hole donor center is detected at 2.2 eV from the CB and the equilibrium Fermi level is pinned at this level. Other localized centers were identified at different positions in the band gap and their relation with the behavior of BTO under different wavelengths and operating conditions is discussed with particular attention to holographic recording. © *2007 American Institute of Physics*. [DOI: 10.1063/1.2434009]

I. INTRODUCTION

Sillenites[1] are quite complex materials exhibiting piezoelectricity, optical activity, and photochromism besides their basic photoconductive and electro-optic properties. Although they do not allow recording large diffraction efficiency holograms they are very suitable for image processing and related applications[2] because of their relatively fast response time and their polarization properties that allow to easily separate diffracted from transmitted beams at the crystal output.[3,4] Their photoconductivity is believed to be of *n* type whereas their dark conductivity is of *p* type. They exhibit light-induced absorption that results in a characteristic photochromic darkening that is more pronounced in $Bi_{12}TiO_{20}$ (BTO) than in $Bi_{12}GeO_{20}$ (BGO) and $Bi_{12}SiO_{20}$ (BSO).[5,6] Sillenites are known to exhibit a large number of photoactive centers in the band gap[7] but their characterization is not a simple task and is still an active research subject.

In this work we report some optical and electrical measurements contributing for a better characterization of the relevant photoactive center levels in BTO. All samples used in this work were grown in the same laboratory in Brazil, using the same procedures and raw chemicals.[8]

Mainly undoped BTO samples with stoichiometric composition $Bi_{12}TiO_{20}$ and thicknesses varying from about 2–3.5 mm were studied which will be generically referred to here as BTO. Some properties of a 1.8 mm thick Pb-doped BTO (570 ppm of Pb) sample which will be labeled BTO:Pb and another sillenite-type $Bi_{12}(Ga_xBi_{1-x})O_{20}$ crystal (labeled BGaO) with $0.6 \leqslant x \leqslant 0.7$ and thickness of 3.5 mm were also measured for comparison. Details for growth of doped crystals are given elsewhere.[9,10]

II. EXPERIMENTS

Pureley electric conductivity, photoconductivity (wavelength-resolved and modulated photocurrent), time-of-flight (TOF), and holographic recording experiments at different wavelengths were performed on some of the samples and the experiments and the corresponding results are described in the following subsections. Data from different experiments are analyzed in order to obtain some information about the localized photoactive states in the band gap of this photorefractive material.

A. Modulated photocurrent measurements

The BTO density of states (DOS) has been investigated via the modulated photocurrent (MPC) technique. Before presenting the results, let us first recall briefly the basic principles of this technique.

The BTO crystal is fitted with two parallel (coplanar configuration) ohmic electrodes on the input crystal surface, polarized with a dc bias, and set on the cold finger of a dynamically pumped cryostat (residual pressure lower than 10^{-4} mbar) so that its temperature can be controlled. It is illuminated by a modulated flux of monochromatic light, the energy of the photons being such that this light induces band to band generation of charge carriers. The time evolution of the flux can be written as

[a]Electronic mail: frejlich@ifi.unicamp.br

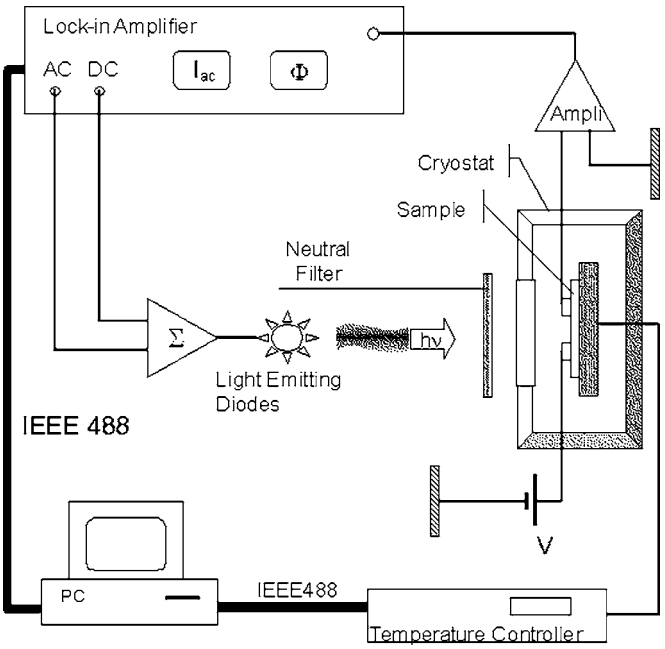

FIG. 1. Sketch of the experimental setup used for MPC measurements.

$$F = F_{dc} + F_{ac}\sin(2\pi ft), \tag{1}$$

f being the frequency of the modulation and t the time. In our experiment the ac flux (F_{ac}) is kept small ($F_{ac} \approx F_{dc}/5$) compared to the dc (F_{dc}) one. To study BTO crystals, whose band gap is of the order of 3.2 eV, the light was provided by a set of nine light emitting diodes (LEDs) having a peak emission wavelength of 380 nm. The advantage of LEDs is that the light emission can be easily controlled by an appropriate polarization (dc+ac) applied to system. At a given temperature T the frequency of the modulation was varied between 12 Hz and 39.9 kHz in 21 values such that $f_{i+1} = 1.5 f_i$. The flux of light, which can be adjusted by the polarization applied to the LEDs, can also be adjusted by means of neutral filters.

With an applied field ξ in between the coplanar electrodes, the ac current I_{ac} resulting from this modulated illumination and flowing in the sample is first amplified by a current/voltage converter ($\times 10^7$) and its modulus and phase shift ϕ referred to the excitation are recorded by a lock-in amplifier which is also used to drive the LED system. All the experiments are computer controlled. Figure 1 presents a sketch of the MPC setup.

It would be too long to recall all the theory on which the MPC spectroscopy is based. The reader can refer to previous publications.[11–13] The physics behind the technique is that the dc flux fixes the recombination process and, consequently, the dc current, whereas the ac current generated by the ac flux reflects the trapping and release processes experienced by the ac generated carriers. We would like to present rapidly below the basic equations used to perform a DOS spectroscopy.

The alternative current I_{ac} measured by the MPC technique gives the quantity NC/μ related to majority carriers

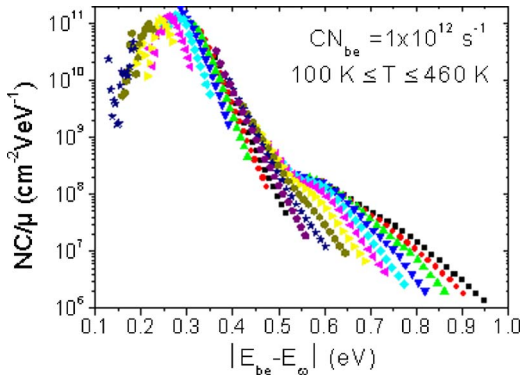

FIG. 2. (Color online) Typical MPC spectra obtained with a BTO crystal. Each set of symbols corresponds to a temperature at which the experiment was performed and, in each set, each symbol corresponds to a given frequency. The MPC technique was performed in the temperature range of 100–460 K in 20 K steps.

characteristics parameters from experimentally known data as, for instance, the ac generation rate G_{ac}, according to the equation

$$\frac{N(E_\omega)C}{\mu} = \frac{2}{\pi k_B T} Sq\xi G_{ac} \frac{\sin\phi}{|I_{ac}|}. \tag{2}$$

In this equation k_B is the Boltzmann constant, q the absolute value of the electron charge, S the cross-sectional area through which the current is flowing, μ the extended state mobility of the majority carriers, and C the capture coefficient of the probed states having a density N at the energy E_ω. A proper energy scaling requires the knowledge of the quantity $N_{be}C$, also called the attempt-to-escape frequency, since E_ω follows from

$$|E_{be} - E_\omega| = k_B T \ln\frac{N_{be}C}{2\pi f} = k_B T \ln\frac{N_{be}C}{\omega}, \tag{3}$$

N_{be} being the equivalent density of states at the band edge E_{be} (bottom of the conduction band or top of the valence band). It can be seen from Eq. (3) that a spectroscopy of the DOS versus energy can be achieved either by changing ω or by changing T. Experimentally we varied both quantities, ω as described above and the temperature in the range of 100–470 K in 20, 10, or 5 K steps. Note that NC/μ and $|I_{ac}|$ are inversely proportional so that the highest the first quantity the lowest the second one.

Figure 2 shows the DOS shape estimated from a measurement with a dc flux $F_{dc} = 10^{14}$ cm^{-2} s^{-1} ($F_{ac} = 2 \times 10^{13}$ cm^{-2} s^{-1}), the product $N_{be}C$ being chosen equal to 10^{12} s^{-1}. In this figure each set of symbols corresponds to a temperature and, in each set, a point corresponds to a frequency: 12 Hz for the deepest in energy and 39.9 kHz for the shallowest in energy, according to Eq. (3). Note that this value of $N_{be}C$ of 10^{12} s^{-1} was chosen at random just to have an overview of the possible NC/μ shape. It can be seen that in the energy range of 0.5–1 eV, NC/μ values are rather low compared to the huge rise of this quantity in the energy range of 0.1–0.5 eV where a peak is clearly distinguishable. The highest values of NC/μ are clearly noisy simply because the I_{ac} values are rather low, in agreement with the remark above on the proportionality of these quantities. That is why this

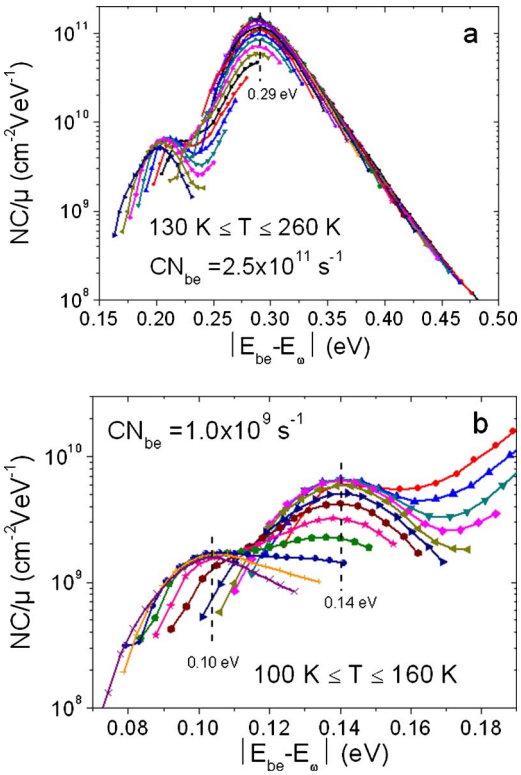

FIG. 3. (Color online) Results of the MPC technique performed with a high flux ($F_{dc}=5\times10^{14}$ cm^{-2} s^{-1}, $F_{ac}=10^{13}$ cm^{-2} s^{-1}). Top figure (a) in the temperature range of 130–260 K in 5 K steps with the choice of $N_{be}C=2.5\times10^{11}$ s^{-1} reveals a peak of states around 0.29 eV. Bottom figure (b) in the temperature range of 100–160 K in 5 K steps with the choice of $N_{be}C=1.0\times10^{9}$ s^{-1} reveals two peak of states around 0.10 and 0.14 eV.

part of the DOS was explored with a higher flux ($F_{dc}=5\times10^{14}$ cm^{-2} s^{-1}, $F_{ac}=10^{13}$ cm^{-2} s^{-1}) and a higher applied field to increase the sensitivity of the experiment.

As shown in a previous paper,[14] a possible method to determine both the energy position and the value of $N_{be}C$ for a given peak consists in adjusting this latter value, i.e., to adjust the energy scale according to Eq. (3), in a way such that several MPC spectra measured at different temperatures and describing this peak are superimposing. With this method the "peak" observed in Fig. 2 was decomposed into three peaks at low energy as shown in Figs. 3(a) and 3(b).

To refine the evaluation of the peak positions, measurements were performed in 5 K steps. Choosing $N_{be}C=2.5\times10^{11}$ s^{-1} it can be seen in Fig. 3(a) that several curves ($\approx$15) are superimposing drawing clearly a peak at an energy of the order of 0.29 eV. These superimposing curves are obtained in the temperature range of 200 K$\leqslant T\leqslant$260 K. For temperatures lower than 200 K, MPC spectra depart from this superimposition but still exhibit a maximum around the same energy position. This departure is due to the progressive modification of the states occupancy linked to an enhancement with decreasing temperature of the quasi-Fermi levels splitting whose energy positions are determined by the dc flux. The trapping states at 0.29 eV are progressively filled (emptied) by the quasi-Fermi levels splitting, if the main carriers are electrons (holes), transforming the trapping states into recombination states that are not probed by the MPC technique.

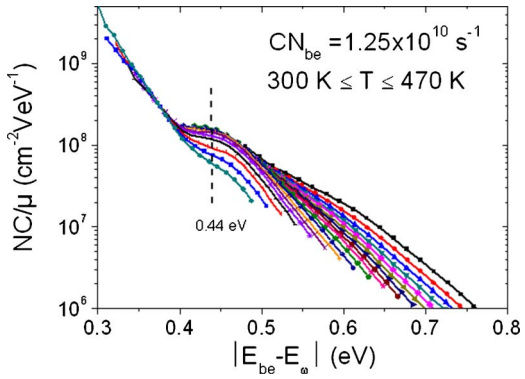

FIG. 4. (Color online) Results of the MPC technique performed with a low flux ($F_{dc}=2\times10^{12}$ cm^{-2} s^{-1}, $F_{ac}=4\times10^{11}$ cm^{-2} s^{-1}) in the temperature range of 300–470 K in 10 K steps. The choice of $N_{be}C=1.25\times10^{10}$ s^{-1} reveals a peak of states around 0.44 eV.

For the lowest temperatures (130 K$\leqslant T\leqslant$155 K) another structure appears described by different MPC spectra the maxima of which are not at the same energy. It means that the $N_{be}C$ chosen for the peak at 0.29 eV is not correct for the shallowest peak observed in Fig. 3(a). A proper choice of $N_{be}C$, such as in Fig. 3(b), aligns the MPC spectra maxima of the shallowest structure of Fig. 3(a) revealing a defect peak at $\approx$0.14 eV. Another peak is observed at lower energy ($\approx$0.10 eV) that seems to have the same capture coefficient as the peak at 0.14 eV.

We have also explored the energy range of 0.5–1 eV with a low flux ($F_{dc}=2\times10^{12}$ cm^{-2} s^{-1}, $F_{ac}=4\times10^{11}$ cm^{-2} s^{-1}) in order to minimize the influence of the dc flux. The final result is shown in Fig. 4 where we have plotted the various MPC spectra with $N_{be}C=1.25\times10^{10}$ s^{-1}.

Clearly a peak of states appears around 0.44 eV described by the superposition of approximately ten MPC spectra. Though it is well reproduced by the superposition of many MPC spectra, this peak is not well shaped (i.e., not as sharp as the previous ones) and appears more as a "foot hill" of a bigger structure, whose onset is seen on the left of the figure, and which is simply the beginning of the very high peak found at 0.29 eV and shown above. Finally, another structure seems to exist deeper in the gap but it is not possible to resolve its position. Table I summarizes the MPC results on undoped BTO. It is worth pointing out that BTO:Pb also exhibits, at least, peaks at 0.29 and 0.44 eV although of roughly tenfold to fifteenfold lower value than for undoped BTO.

Before ending this section we would like to say a word about the precision on the determination of some of the peaks parameters with the method we used above. When

TABLE I. DOS for BTO.

$\lvert E_\omega - E_{be}\rvert$ (eV)	NC/μ ($10^9\times$ V/cm^2)	$N_{be}C$ ($10^9\times$ s^{-1})	$NC/\mu/(N_{be}C)$ (V s/cm^2)
0.10	1.5	1.0	1.5
0.14	7	1.0	7
0.29	110	250	0.4
0.44	0.11	12.5	0.01

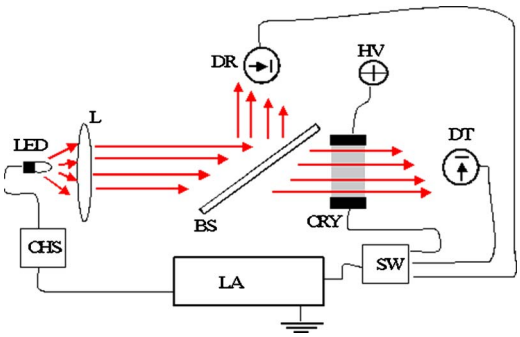

FIG. 5. (Color online) Wavelength-resolved photocurrent measurement setup: LED source of light illuminating the sample CRY by a collimating lens L and electronically chopped at frequency f (f=200 Hz in this case) by the chopped source (CHS) driven by the reference oscillator of the lock-in amplifier (LA). The latter is used for the measurement of the photocurrent through transverse electrodes by the side of the crystal sample and fed by a dc high voltage (HV) source. The transmitted and incident [sampled by the beamsplitter plate (BS)] irradiances are detected by photodetectors DT and DR and measured by the lock-in amplifier. The switch (SW) allows sequentially feeding the lock-in amplifier with the photocurrent and the signals from photodetectors for measurement. Different LEDs covering the wavelength measurement range are rotated in the setup using a stepping motor. The whole experiment is controlled by a computer.

peaks are clearly detected such as those presented in Fig. 3 the determination is rather accurate. However, the $N_{be}C$ value we use enters in a logarithmic energy scaling. Thus, if we assume that this quantity is fixed within a factor of 2, it results in an error of the order of 10 meV $[k_BT\ln(2)]$ on the energy position at a temperature of 200 K. For structures such as the one described in Fig. 4 the error is slightly higher. A decrease by a factor of 4 of the $N_{be}C$ used to plot the MPC spectra results in an energy position of the peak shifted by 20 meV downward. With such a decrease of $N_{be}C$, we still obtain a superposition of the MPC spectra though slightly worse. In conclusion, we believe that the $N_{be}C$ we found are determined within a factor of 2–4 and the energy positions with an error of the order of 10–20 meV.

B. Wavelength-resolved photoconductivity

Wavelength-resolved photoconductivity (WRP) is a powerful tool for detecting localized levels in the band gap. It is a complementary technique for MPC because the latter detects unpopulated levels whereas WRP detects only (at least partially) populated ones. The experiment is carried out using discrete sources of light provided by almost monochromatic LEDs as schematically depicted in Fig. 5 and using electrodes on the lateral faces (transverse configuration) of the samples in order to collect all the current generated in the volume of the sample. The current is measured using a lock-in amplifier synchronized with the frequency-modulated light shining the sample in order to get rid of currents that are not associated to the light. More details about the apparatus and the technique are described elsewhere.[15]

The technique requires the measurement of the effective absorption coefficient in order to compute the light distribution (and associated photocurrent) in the sample's thickness. A photocurrent coefficient $\underline{\sigma}$ results from

$$\underline{\sigma} \equiv h\nu\frac{\sigma_{ph}(0)}{I(0)} = q\mu\tau\Phi\alpha, \tag{4}$$

which is computed from the experimental quantities

$$\underline{\sigma} = \frac{i_{ph}}{HD}\frac{\ell}{V}\frac{h\nu}{I(0)}\frac{\alpha D}{1-e^{-\alpha D}}, \tag{5}$$

where i_{ph} is the measured photocurrent, ℓ the interelectrode distance, D and H the sample's thickness and height, respectively, $I(0)$ the irradiance at the sample input plane inside the sample, V the applied voltage, α the irradiance absorption coefficient, q the absolute value of the charge of the electron, μ and τ the mobility and lifetime of the photoexcited charge carrier in the extended states, and Φ the quantum efficiency of charge carrier photogeneration. The αD term above is computed from the experimentally measured signals from photodetectors DR and DT in Fig. 5.

The optical transitions giving rise to a current are either transitions from the valence band (VB) states to empty, or at least partially empty, defect states, leading to hole generation, or transitions from filled, or at least partially filled, defect states towards the conduction band (CB), leading to electron generation. Increasing the photon energy introduces new transitions and each of them results in an increase of the current so that an upward step in $\underline{\sigma}$ should be detected.

All experiments showed a transient behavior, at least in certain wavelength range, characterized by a large initial photocurrent rapidly decaying to a stable stationary value. We believe such a behavior arises from inverse polarization due to space-charge shielding. In fact, it is practically impossible to avoid some parts of the sample to be less illuminated, mainly near the electrodes. In these darker regions the photoconductivity σ_{ph} is lower and the electric field ξ is correspondingly higher in order to keep the current density $j=\sigma_{ph}\xi$ constant. In the region where the illumination changes, ξ does change too and according to the Maxwell's equation

$$\epsilon\varepsilon_0 \nabla \cdot \boldsymbol{\xi} = \rho \tag{6}$$

there should be an accumulation of electric charge there. Charges of opposite sign accumulate on the opposite dark-to-bright and bright-to-dark regions along the interelectrode direction and these charges produce a space-charge field opposing the externally applied field. Such an electric polarization was, in fact, detected in our experiments with BTO. This polarization is a rather slow effect because it depends on charge transport in the sample's volume which is controlled by the so-called Maxwell or dielectric relaxation time. It is therefore possible to reduce the effect of electric charges polarization by measuring the photocurrent at the very beginning before charges are able to sensibly diffuse. Also, the illumination is kept on without applied electric field for a sufficiently long time in between two successive measurements in order to allow the accumulated charges to diffuse away. All data in this paper were obtained following this procedure.

The following different WRP experiments were carried out:

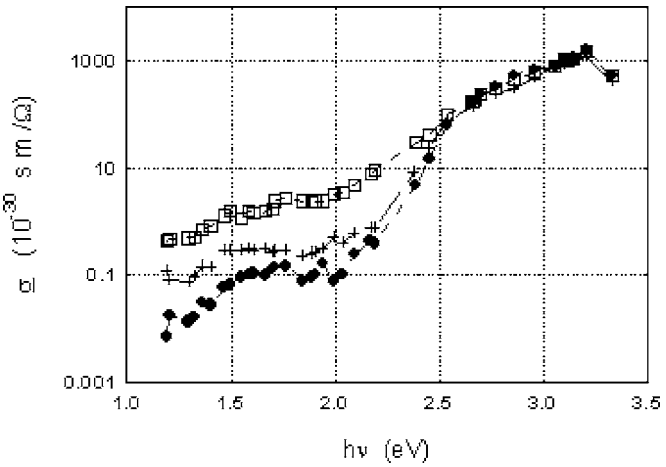

FIG. 6. Photocurrent coefficient measured as a function of the photon energy on undoped BTO:WRP/R (●), WRPeq/N (+), and WRPpre (□).

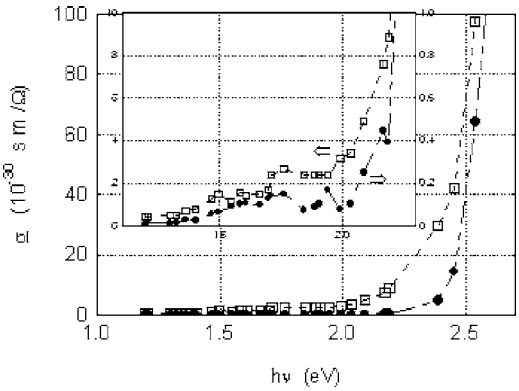

FIG. 8. Expanded view and inset of σ in Fig. 7 showing steps that are rather clear for the preexposed WRPpre (□) experiment and rather weak or difficult to detect for the relaxed WRP/R sample (●) at 1.3, 1.4, 1.7, and 1.9 eV. Other steps at 2.0, 2.2, 2.4, and about 2.5 eV are neatly detected in both experiments.

- WRP: Means the photocurrent measured from lower to higher photonic energies with LEDs at their maximum possible power in the setup.
- WRPpre: Same as before but with the sample being preexposed for at least 30 s with a given radiation (in this paper it was always with $h\nu$=2.4 eV) immediately before any measurement, that is to say, before measuring the light irradiance with photodetectors DT and DR, and before measuring any of the successive i_{ph} at each different voltage for each one of the different wavelengths in the spectral range.
- WRPeq: Measurement carried out from lower to higher photonic energies but with all LEDs being fixed at a preselected value of photonic flux (photons per unit surface and unit time). The LEDs with a maximum flux lower than the selected one are also included in the run, as well, with their maximum available flux.

The above experiments were carried out on samples in the following different conditions:

- "Relaxed:" The sample was kept for a couple of hours in the dark at 80–90 °C for achieving a thermal equilibrium of the charge carriers population in the localized states in the band gap. This temperature was shown to partially relax optically excited deep traps in undoped BTO but is not high enough to bring them to full thermal equilibrium.
- "Normal:" The sample has already been submitted to at least one full spectral range measurement run in the last couple of days and was not submitted to any special treatment for relaxation. Although normal state is not well defined, it is relevant because it represents the actual state of the sample in current applications.

In the following we will use a notation summarizing both the type of experiment and the state of the sample such as WRPeq/R for the case of an equalized photonic flux (WRPeq) on a (partially) relaxed sample. A simple WRP experiment on a normal sample, for example, will be labeled WRP/N and so on. For experiments with preexposition at $h\nu$=2.4 eV the results do not depend on the state of the sample so that they will be simply labeled WRPpre.

1. BTO

Measurements were carried out mainly on undoped BTO and also on BTO:Pb and BGaO for comparison. Results for undoped BTO are reported on a semilog scale in Fig. 6 to get

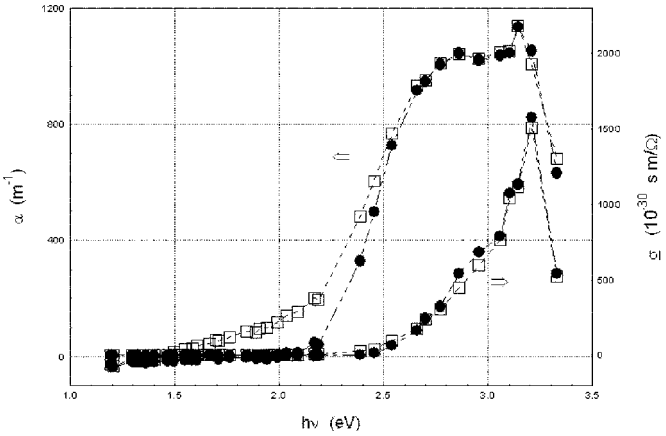

FIG. 7. Photocurrent coefficient (right-side axis) and absorption coefficient (left-side axis) measured as a function of the photon energy on undoped BTO for WRP/R (●) and WRPpre (□).

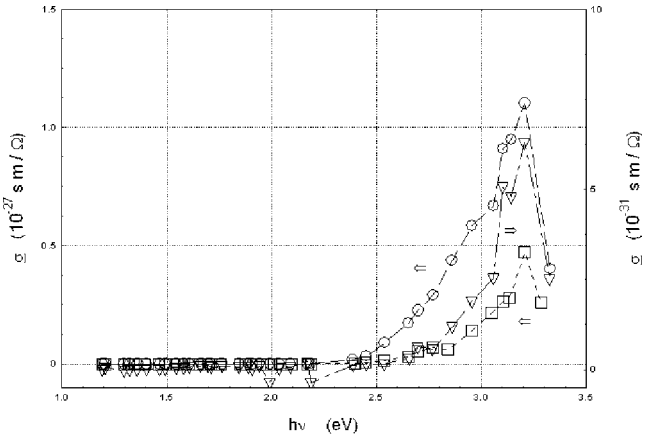

FIG. 9. Photocurrent coefficient measured for different photon energies in WRP/N regimes for BGaO (▽) for BTO:Pb (□) and for undoped BTO (○).

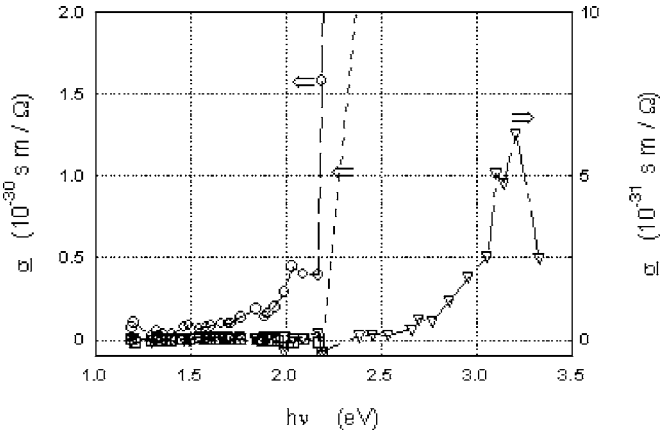

FIG. 10. Expanded view of the photocurrent coefficient in Fig. 9: WRP/N regime for BGaO (▽), BTO:Pb (□), and undoped BTO (○).

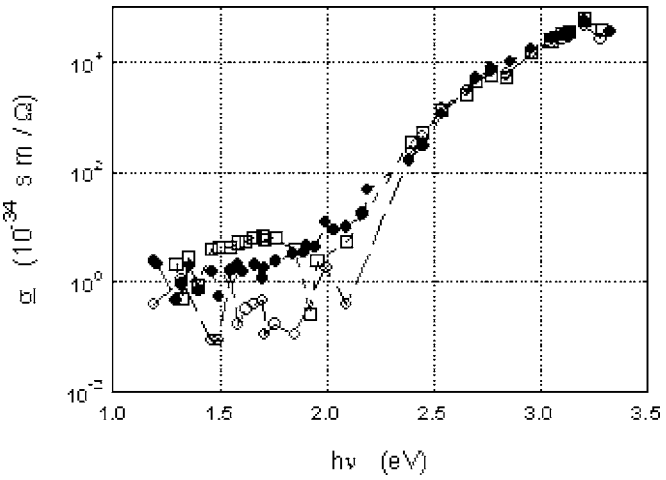

FIG. 11. Photocurrent coefficient measured as a function of photon energy on BTO:Pb in WRPpre (□), WRP/N (○), and WRPeq/N (●) regimes.

a general overview. There we see that the photocurrent coefficient $\underline{\sigma}$ measured with preexposure (WRPpre) is roughly fivefold larger than measured in normal conditions (WRPeq/N) and fiftyfold larger than for the relaxed sample (WRP/R) in the low energy range of 1.2–1.3 eV. At $h\nu = 2.0$ eV the preexposed photocurrent coefficient is about sevenfold larger than for the normal sample and thirtyfold larger than for the relaxed one whereas these relations are 12 and 25, respectively, at $h\nu = 2.2$ eV. From $h\nu \approx 2.5$ eV on, all three curves exhibit roughly similar values for $\underline{\sigma}$. Measuring with equalized flux (WRPeq) or not (WRP) did not show significative differences for BTO.

Figure 7 shows the photocurrent $\underline{\sigma}$ coefficient together with the corresponding absorption coefficient α for a preexposed (WRPpre) and a relaxed (WRP/R) sample with the following relevant features:

- Both curves show a sharp peak at 3.2 eV for $\underline{\sigma}$, corresponding to the band gap edge.
- The absorption curves are somewhat "rounding," instead of sharply increasing, as they approach the band gap edge. The rounding of the absorption coefficient near the band gap edge is probably due to the presence of luminescence effects that are detected in this setup because the transmitted light is measured using a photodotector placed close (about 15 mm) to the rear face of the sample. From the shape of the absorption coefficient curve it seems that photoluminescence may be quite relevant from about 2.7 eV on, so that photocurrent data in this range may not be reliable because it cannot be directly related to the incident radiation.
- Relaxation and preexposure are clearly affecting the absorption coefficient (and the photocurrent too, as observed in the previous and following graphics) mainly in the 1.2–2.4 eV range, as expected. The steps in the photocurrent coefficient in Figs. 6–8 indicate the presence of populated photoactive centers at least at 1.3, 1.4, 1.7, 1.9, 2.0, 2.2, 2.4, and 2.5 eV. The one at 2.2 eV is the only one that is sharper for the relaxed sample than for the preexposed one (probably because of the higher contribution of the nearby levels in preexposed samples) thus indicating it is the lowest energy level which is not affected by temperature relaxation and is likely to be the one characterizing the Fermi level. This value is in agreement with data in the literature indicating the Fermi level to be about 1 eV above the VB or 2.2 eV below the CB. All other steps detected below 2.2 eV are strongly enhanced by

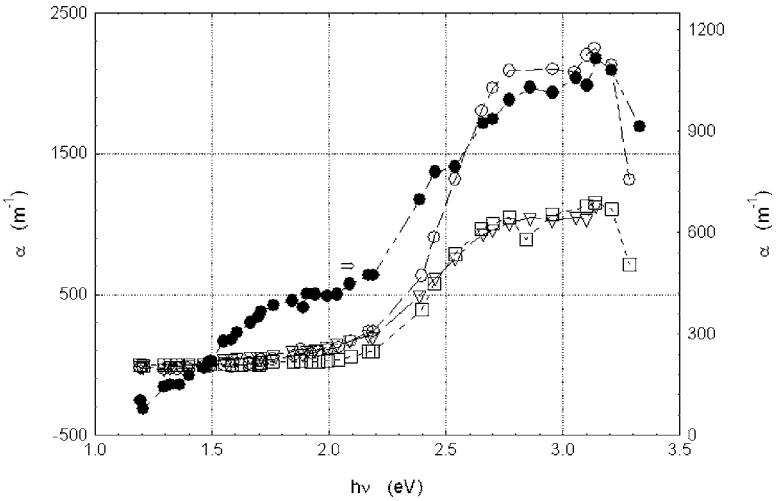

FIG. 12. Irradiance absorption coefficient vs photon energy measured close to the sample for undoped BTO (□ for thermally relaxed, ▽ for preexposed light) and BTO:Pb (○), all on the left-side axis, and for BGaO (●) on the right-side axis.

preexposure at 2.4 eV so that we believe they are between the Fermi level and the CB. These levels are partially populated probably by pumping electrons from the VB and/or states below the Fermi level upon illumination with energetic photons in previous experiments or because of preexposure. These levels in the 1.3–2.0 eV range are able to store electrons for a time long enough to record holograms, as will be reported in Sec. II D. For energies higher than 2.6–2.7 eV the photocurrent is rather monotonically growing and it is not possible to clearly identify discrete steps, probably because of the photoluminescence effects we have already mentioned before.

2. Doped BTO

Figure 9 exhibits a similar broad shoulder in $\underline{\sigma}$ near the band edge, with a sharp peak at 3.2 eV, for BTO:Pb, BGaO, and BTO. The peak at 3.2 eV is roughly 10^{-4}-fold lower for BGaO.

The expanded view in Fig. 10 does not show steps in $\underline{\sigma}$ for BGaO in the 1.2–3.2 eV range except at about 2.7 and 2.8–2.9 eV. This figure also does not show steps in $\underline{\sigma}$ for BTO:Pb from 1.2 eV until the sharp step at 2.2 eV and the steadily increasing curve from this point on. Also noticeable is the lack of a step at 2.0 eV which is always present and rather large for BTO. Figure 11 shows that the effect of preexposure on BTO:Pb is much weaker than for BTO. Influence of the preexposure is only visible around 1.5 eV where $\underline{\sigma}$ is clearly higher for the WRPpre measurement than for the other experiments. This fact indicates that either the distribution of states in the 1.2–2.2 eV range is different in BTO:Pb compared to BTO, with almost no states in the range of 1.7–2.0 eV, or that, if the distribution is the same, these states are rapidly relaxing.

Figure 12 shows the irradiance absorption coefficient measured for undoped and doped BTO but the reader should keep in mind that these curves are affected by luminescence effects, as discussed above. It is interesting to note a broad absorption band at about 1.8 eV for BGaO that is absent on BTO:Pb and undoped BTO. This peak is believed[16] to have no relation with BGaO itself but with contamination with Mn and Ca. In any case the absorption curves themselves, although necessary for photoconductivity data processing, do not seem to bring about much information about localized states of sillenites.

C. Light-induced absorption

Photochromism in sillenites is believed to arise from the electron filling of initially empty shallow traps (St) by the action of light during optical recording in Dt (deep traps) and is adequately described by the so-called two-center model.[17] The thermal relaxation of these filled shallow traps is rather slow so that the associated photochromic effect remains for some time even in the dark. The density of these St is usually much lower than that of Dt so that they can be easily saturated. In spite of their lower density, their darkening effect is rather pronounced probably because of their comparatively large effective photon cross section. BTO crystals undergo strong light-induced photochromic darkening with radiation in the visible wavelength range and darkening with 514.5 nm wavelength light, for example, is noticeable in nominally undoped and Pb-doped BTO for as low an irradiance as a few $\mu W/cm^2$.[5] Such an effect was also verified at least on undoped BTO using light in the wavelength range of 514.5–633 and even 780 nm, but not with 1064 nm.[18] The activation energy of these St centers involved in photochromic effect was measured from absorption relaxation decay time in the dark at various temperatures (using the Arrhenius technique) and reported[18] to be $E_{ST}=0.42\pm0.02$ eV, presumably below the CB, for undoped BTO.

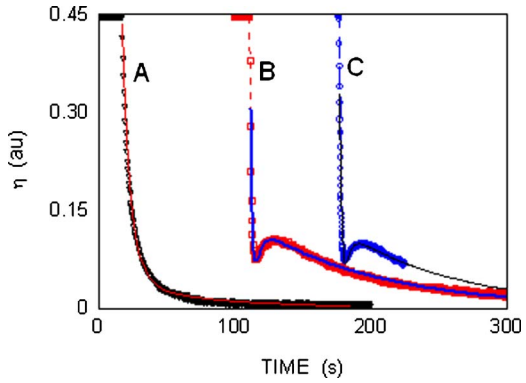

FIG. 13. (Color online) Erasure of a hologram in BTO:Pb recorded with 633 nm beams and erased with one of the recording beams: (**A**) without preexposure; (**B**) and (**C**) same as for (**A**) but preexposed with a spatially uniform $\lambda=532$ nm light illumination for a few minutes before starting (after preexposure switching off) 633 nm recording. Curves (**B**) and (**C**) are the curves measured along each one of the incident beams. All three curves are artificially shifted in time for better observation. Data for (A) (▽) is fitted (full line) by a couple of in-phase exponentials whereas (**B**) and (**C**) data (□ and ○) are fitted (full line) by a couple of counterphase exponentials. Same experiment on undoped BTO always leads to a monotonically decreasing η.

D. Photorefractive recording

Photorefractive recording in undoped sillenites is predominantly associated to *n*-type photoconductivity.[19] Holograms are known to be easily recorded on undoped BTO with light at least in the visible 514.5 nm (2.4 eV)–633 nm (1.96 eV) wavelength range. The holographic recording in

TABLE II. Fitted parameters from holographic erasure on BTO:Pb with 633 nm.

Curve	Preexposed	A (Arbitrary unit)	B (Arbitrary unit)	B/A	τ_{sc}^{A} (s)	τ_{sc}^{B} (s)	$\tau_{sc}^{B}/\tau_{sc}^{A}$	φ (rad)
A	No	0.27	0.34*	1.26	5.9	37	6.3	···
B	532 nm	0.71	−0.36	−0.51	3.6	184	51	0.87
C	532 nm	0.72	−0.35	−0.49	3.2	172	54	0.89

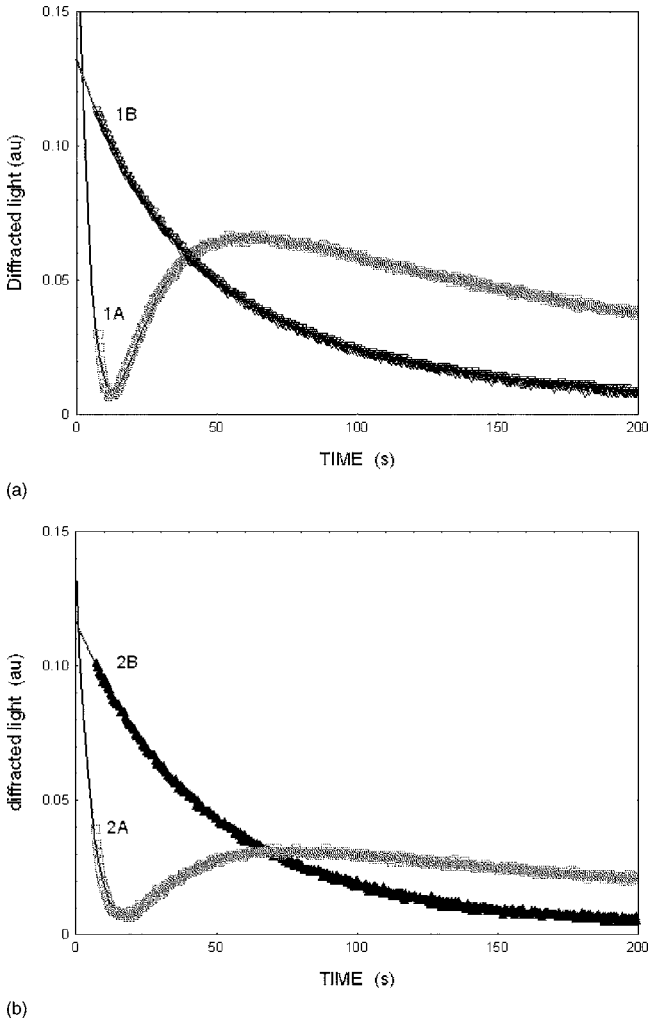

FIG. 14. Erasure of holograms in BTO:Pb recorded during 2 min with a laser diode of 780 nm wavelength, observed along the reference beam direction (upper graph) and along the signal beam (lower graph). The curves showing a local maximum result from 3 min preexposure at 524 nm light from a LED. The monotonically decreasing curves are without preexposure.

undoped BTO with $\lambda = 780$ nm (1.59 eV) and $\lambda = 1064$ nm (1.16 eV) with visible light preexposure[7] was already reported.

1. Direct recording

Nonpreexposed holographic recording in the range of 514.5–633 nm was carried out for BTO and BTO:Pb that always showed predominantly *n*-type holograms on more than one photoactive center as already reported elsewhere[18] for BTO and Pb-doped BTO, and shown here for 633 nm on BTO:Pb in curve A of Fig. 13. The latter curve was fitted with

$$\eta = \left| A e^{-t/\tau_{sc}^{A}} e^{i\varphi} + B e^{-t/\tau_{sc}^{B}} \right|^2 \tag{7}$$

and the corresponding parameters are reported in Table II. These results indicate that at least two different deep trap photoactive centers are involved in photorefractive recording with 633 nm. Similar results had been previously reported[20] for $Bi_{12}GeO_{20}$ and $Bi_{12}SiO_{20}$.

Recording with 780 nm also showed predominantly *n*-type holograms in BTO and Pb-doped BTO. However, although not conclusive for BTO, hologram erasure on BTO:Pb clearly shows a monoexponential curve (see curves 1B and 2B in Fig. 14) thus indicating that 780 nm recording involves a single photoactive center at least for Pb-doped BTO. These monoexponential curves were very accurately fitted with Eq. (7) with $B=0$ and the resulting parameters are reported in Table III.

2. Preexposed recording

Preexposed BTO samples either undoped or Pb-doped were shown to exhibit hole-electron competition. Such a competition is evidenced in holographic recording experiments when *n*-type and *p*-type holograms occur to be recorded on different localized states. In this case counterphase holograms are obtained, also exhibiting different recording time constant and a very characteristic shape[21,22] upon erasure. When *n*- and *p*-type carriers do contribute to the recording on a single photoactive level, instead, either electrons or holes predominate and the erasure is always monotonically decreasing as if one single charge carrier was involved.

Hole-electron competition occurs under the following slightly different conditions for undoped and Pb-doped samples:

- Undoped BTO: Recording with 780 nm (1.59 eV) and preexposure using uniform light with $h\nu \geqslant 2$ eV, as reported elsewhere[21] always leads to an erasure hologram curve typically characterizing the simultaneous presence of *n*-type and *p*-type holograms in different photoactive centers. Instead, preexposure with photonic energy lower than 2 eV or recording with $h\nu \geqslant 2$ eV with or without preexposure always leads to a monotonically decreasing hologram erasure curve.
- Pb-doped BTO: Holograms were recorded and erased with the same light, using a 633 nm (1.96 eV) laser with 532 nm (2.33 eV) or shorter wavelength preexposure. In this case erasure exhibits the typical hole-electron competition shape observed in Fig. 13 (curves B and C). Same experiment with same preexposure was carried out on BTO:Pb but recording and erasing with 780 nm (1.59 eV) and also showed a typical hole-electron competition as shown in Fig. 14 (curves 1A and 2A). All curves exhibiting hole-electron competition (curves B and C in Fig. 13 and curves 1A and 2A in Fig. 14) were also fitted with Eq. (7) and the resulting parameters are reported in Table II for 633 nm recording and in Table III for 780 nm recording. In these cases A and τ_{sc}^{A} represent *n*-type holograms and B and τ_{sc}^{B} represent *p*-type holograms, where the minus sign in B indicates that they they are opposite sign holograms. The parameter φ is a random phase shift probably arising from environmental perturbations. This phase shift perturbation is likely to occur in hole-electron competition because of the very large difference in their characteristic recording time.

TABLE III. Fitted parameters from holographic erasure on BTO:Pb with 780 nm.

Curve	Preexposure	A (Arbitrary unit)	B (Arbitrary unit)	B/A	τ_{sc}^{A} (s)	τ_{sc}^{B} (s)	$\tau_{sc}^{B}/\tau_{sc}^{A}$	φ (rad)
1A	524 nm	0.72	−0.30	−0.72/0.3	13	461	35.5	−0.34
1B	No	0.34	⋯	⋯	98	⋯	⋯	⋯
2A	524 nm	0.54	−0.21	−0.54/0.21	15.3	556	35	0.43
2B	No	0.332	⋯	⋯	97	⋯	⋯	⋯

3. Dark relaxation

Holographic dark relaxation is controlled by the conductivity in the dark. The study of the diffraction efficiency decay in the dark of a previously recorded (with $\lambda=514.5$ nm light) hologram, as the one shown in Fig. 15, was already reported elsewhere[18] and carried out at different temperatures in order to compute its associated activation energy from an Arrhenius plot. This activation energy resulted to be about 1 eV, presumably above the VB because conductivity in the dark is known to be of p type. This value is in agreement with previously reported values of 1.1 eV,[1,23] 1.06 eV,[6] and 0.99 eV,[24] among others. Note that relaxation in Fig. 15 perfectly follows a monoexponential decay instead of a double exponential as it is the case in light-erasure experiments. This fact is in agreement with the model of dark erasure occurring via a single hole-donor level, which is probably the Fermi level at about 1 eV above VB.

Direct electric conductivity in the dark was also measured at different temperatures on an undoped BTO sample with golden electrodes evaporated on one of the crystal faces (coplanar configuration) and separated by approximately 2 mm. An Arrhenius-type plot of these data is reported in Fig. 16 where one curve is for increasing and the other for decreasing temperature from which data of an activation energy of 0.85 eV are computed. This value however, is sensibly lower than those already reported in the literature by other researchers for this material and also lower than the one obtained from holographic dark relaxation and reported above.

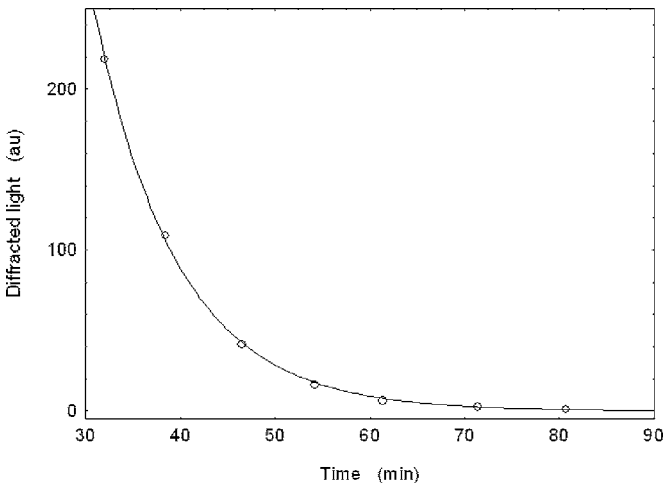

FIG. 15. Diffracted light measured during dark relaxation in a hologram previously recorded in an undoped BTO. Measurement is carried out using short pulses of the same $\lambda=514.5$ nm beams used for recording. Data (○) are fitted by a monoexponential decay curve (full line).

E. Time of flight

Time of flight (TOF) allows the determination of the trap-limited mobility or drift mobility μ_D of charged carriers and has already been used for sillenites before.[25] The experiment was carried out for Pb-doped and undoped BTO using a short (3–4 ns) pulse of UV light illuminating just the surface of the sample in contact with one of the electrodes while the sample was kept under steady and uniform illumination of green (525 nm) or blue (430 nm) light. Indeed it was impossible to record a transient for the sample being maintained under dark or even under steady red (630 nm) illumination. The applied field in between the electrodes was chosen such that we recorded the drift of electrons. TOF experiments led to electronic mobilities $\mu_D \approx 0.16$ and ≈ 1.6 cm^2 V^{-1} s^{-1} referred to room temperature for BTO and BTO:Pb, respectively. On the other hand we have reported above (Sec. II A) a roughly tenfold to fifteenfold lower DOS for BTO:Pb than for BTO. Considering that μ_D and DOS are roughly inversely proportional to each other, these data are clearly consistent.

III. DISCUSSION

Photoconductivity experiments confirmed the well known band gap of 3.2 eV for all the studied crystals, in

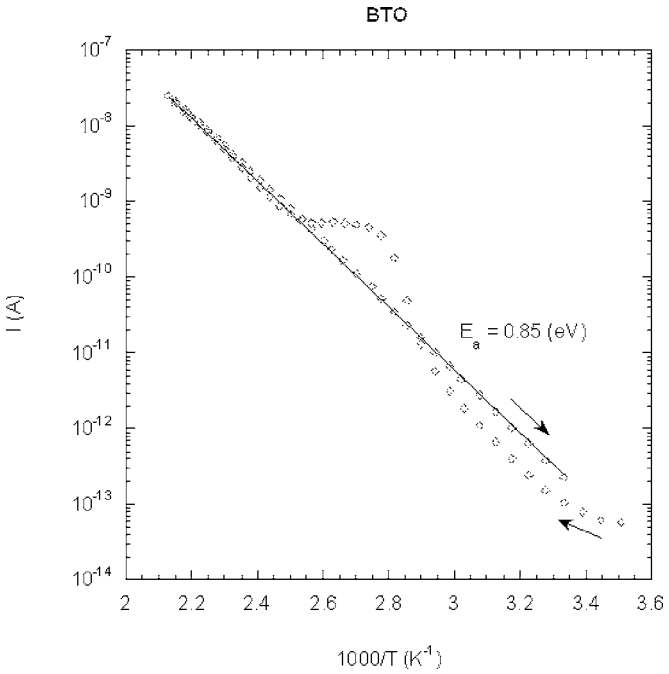

FIG. 16. Arrhenius plot of dark photocurrent measured on an undoped BTO both for increasing (up arrow) and decreasing (down arrow) temperature.

agreement with the band gap being known to mainly depend on the Bi–O bond and not on Ga or Ti. However, these measurements showed that the BGaO crystal presents some properties rather different from the two others. We shall come back to this crystal later. Both on the BTO and BTO:Pb the MPC technique reveals peaks of localized states around 0.1, 0.14, 0.29, and 0.44 eV, probably below the CB, these last two peaks being less intense by a factor of say 12 in the BTO:Pb material.

Photoconductivity measurements performed with photon energy in the range of 1.2–3 eV reveal a localized state at 2.2 eV, presumably below the CB, which is likely to be responsible for the pinning of the Fermi level E_f in both BTO and BTO:Pb crystals. Several other states were detected—they were particularly visible with the undoped BTO crystal—and attributed to levels of states in between E_f and the CB because they were apparently empty under equilibrium after thermal relaxation. Some filled states in between E_f and the VB were also detected but not accurately separated into discrete levels because of the limitations of our WRP technique.

Electrons can be optically pumped to fill in centers in the 1.2–2.2 eV range, probably below the CB, that relax to equilibrium within hours in the dark for undoped BTO. In fact, dark electric conductivity showed quenching (in growing temperature runs) effects over conductivity in BTO (see Fig. 16) thus indicating that out-of-equilibrium distribution of charge carriers does persist for some time after illuminating the sample. In BTO:Pb we did not detect as much centers as in BTO in the same range of energy. It may exist some levels around 1.5 eV, also probably below the CB, put into evidence by the WRPpre experiment, but with a lower density than in undoped BTO, since the WRPpre signal was smaller in BTO:Pb than in BTO. The fact that BTO:Pb presents less states or less dense levels than in BTO is underlined by the higher overall optical absorption coefficient we observe in Fig. 12 in the Pb doped material near the band edge. Indeed, less localized levels results in less larger wavelength (less absorbed) radiative relaxation of the photocarriers from the extended to the localized states thus promoting band-to-band shorter wavelength (more absorbed) radiative recombination instead. Despite the evidences that BTO:Pb exhibits less states or less dense states than BTO, deep states are present in both materials that limit the electron transport. The presence of these deep states, well below the CB, is probably the reason why we had to illuminate the crystals of BTO and BTO:Pb with a steady green or blue light to observe clear transient signals in the TOF experiment. We think that by doing so we filled these deep levels that become less active for trapping the carriers while they drift through the material.

Holographic experiments, only possible for BTO and BTO:Pb, showed that, without preexposure, recording is predominantly of n type (electrons) and likely to occur mainly around the Fermi level and in at least one more level. Recording is believed to rely mainly on $Bi^{3+}+h^+$ centers, occupying Ti^{4+} vacancies, that are at the same time donors ($Bi^{3+}+h^++h\nu \rightarrow Bi^{5+}+e^-$) and acceptors ($Bi^{3+}+h^++e^- \rightarrow Bi^{3+}$) thus enabling the building up of the necessary space-charge modulation for holographic recording. Recording is also possible even with photon energy much lower than 2.2 eV (for instance, 1.59 eV, $\lambda=780$ nm), the energy gap between E_f and the CB. Such a recording cannot be based on a two-photon recording mechanism because the recording beams are relatively weak. It is therefore likely that a two- or multiple-step mechanism involving more than one localized level in the band gap has to be considered. A possible explanation is that the electrons are first optically pumped to one—or more—intermediate levels from the occupied levels located below the Fermi level and then excited to the CB and redistributed in these states to record the hologram. The intermediate states concerned are probably those in the energy range of 1.3–1.5 eV below the CB detected by the WRPpre experiment. They cannot be deeper in the gap otherwise transitions from these intermediate levels and the CB, essential for electrons distribution during hologram recording, would not be possible for a wavelength of 780 nm.

Simultaneous n-type and p-type holograms are recorded in different levels but only with preexposure. A possible explanation may be that preexposure may pump electrons from the Fermi into other levels where n-type holograms are recorded and at the same time a sufficiently large amount of holes are left behind in the Fermi level to enable the recording of a predominantly p-type hologram on it. Preexposure simultaneous n-type and p-type holograms are easier to occur in BTO:Pb than in BTO and we may speculate about this fact being due to a lower density of electron donors in BTO:Pb that would facilitate their relative "exhaustion" during preexposure. The lowering in the density of donors in BTO:Pb may occur by the Pb^{4+} (that are not photoactive) occupying some of the Ti^{4+} antisites thus reducing the number of $Bi^{3+}+h^+$ (donors) in these antisites.

The monoexponential hologram relaxation in the dark (see Sec. II D 3) is confirming the widespread model of a single species (holes in the Fermi level at 0.85–1 eV above the VB) being responsible for dark erasure in sillenites. Decreasing temperature runs of dark photoconductivity in Fig. 16 showed a Fermi level at 0.85 eV (presumedly above the VB) which is somewhat lower than the 0.95–1.05 eV reported in the literature using different techniques and also deduced from our photoconductivity measurements showing a huge step at 2.2 eV (or 1.0 eV above the VB).

Slowly decaying photochromic effect was detected in BTO and BTO:Pb. The activation energy for this effect turned to be 0.42 eV as measured for BTO. We may be tempted to believe that this one is the same 0.44 eV level already reported from MPC experiments in spite of the latter technique being unable to detect slowly decaying states that is the case of photochromic centers here.

It is worth remarking that we were unable to record a hologram in BGaO and there were no localized states detected in the 1.2–2.2 eV range. These two facts are consistent with our assumption that donor states in this range are necessary for n-type holographic recording. We may therefore think of BGaO as a structure similar to BTO where all Ti^{4+} are substituted by $Ga^{3+}+h^+$ (electron acceptor) thus reducing the density of $Bi^{3+}+h^+$ (donors and acceptors) occupying these sites and thus preventing holographic recording. This hypothesis is consistent with the 10^5-fold higher dark

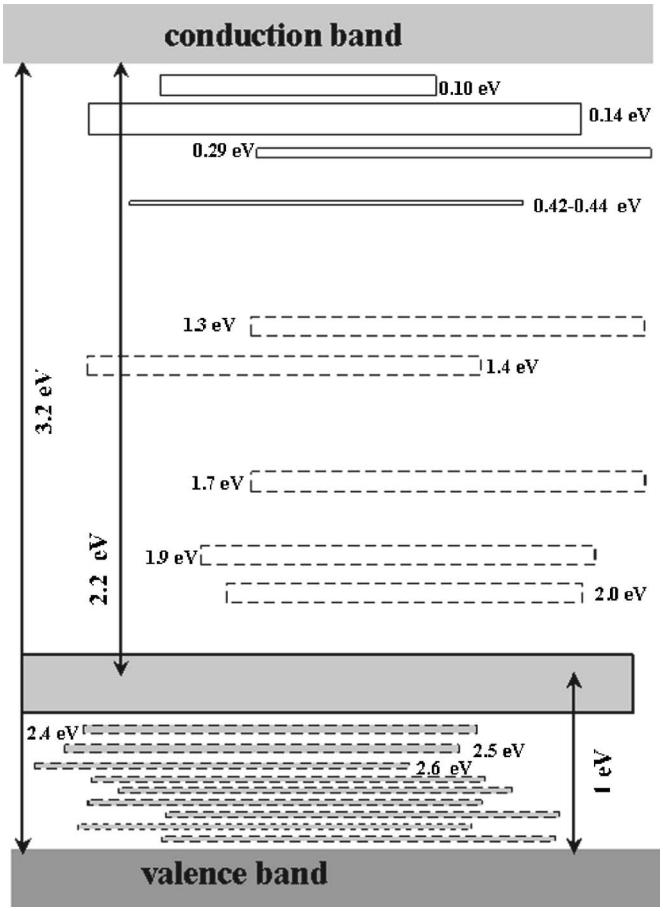

FIG. 17. Schematic representation of photoactive levels in the BTO band gap, with energies measured from the bottom of the CB. Filled electron-donors are in gray and empty levels in white. The DOS is qualitatively represented by the width of the full-line limited levels whereas the dashed-line limited ones are not. The succession of states close to the VB represent the almost continuous localized states distribution at this position with a few discrete ones at 2.4, 2.5 and 2.6 eV.

(probably hole-based) conductivity exhibited by BGaO and Ga-doped BTO (Ref. 5) compared to BTO. If this Ga-based acceptor level is closer than 1.2 eV from the VB we would not have been able to detect it with WRP experiments as it was probably the case here. We shall also recall that recording holograms requires the simultaneous presence of electron donors and acceptors inside the band gap in order to be able to redistribute electric charge carriers under the action of light. This is possible on BTO and BTO:Pb because of the presence of $Bi^{3+}+h^{+}$ (donor and acceptor) but is certainly not the case of BGaO.

The analysis of the data from experiments reported in this paper as well as from recent publications about similar BTO samples and discussed above seems to lack of a conclusive picture about the distribution of photoactive centers in the band gap of this material. This is probably due to the fact that there is not a "unique" BTO and that from one crystal to another, depending on the preparation, some defects may predominate over others. It is therefore not surprising that from one crystal to some other one we found different results. Nevertheless, considering the undoped BTO and BTO:Pb, we have shown that for both materials the Fermi level was pinned around 2.2–2.3 eV below the CB. In addition, the MPC technique reveals the same levels, probably close to the CB, with different densities, the ratio of which is corroborated by the ratio of the TOF mobilities we determined. The WRPpre experiments showed that the same levels around 1.3–1.5 eV are also present in both crystals in smaller density in the BTO:Pb than in BTO. These levels are likely to be those involved in hologram recording either only *n* type or both *n* and *p* types without and with preexposure, respectively. Hence, BTO and BTO:Pb are not as different in terms of defect levels as it could appear at first sight and we have summarized in Fig. 17 the various levels that could be encountered in these crystals. Of course it is clear that more work is needed to decide if these results are so general that they could apply to any BTO crystals. We shall take advantage of the present results to compare these BTO crystals with other materials, as we did here with BGaO, putting into evidence that differences in density of defect levels are reflected by very different behaviors in terms of charge carriers transport properties from one type of crystal to another.

IV. CONCLUSIONS

The analysis of the data from experiments reported in this paper as well as from recent publications about similar BTO samples and discussed above is still not able to provide a conclusive picture about the distribution of photoactive centers in the band gap for this material. The diagram in Fig. 17 is one, among other possibilities, that may account for many features of BTO.

ACKNOWLEDGMENTS

This work was partially supported by the Conselho Nacional de Desenvolvimento Científico e Tecnológico-CNPq and the Fundação de Amparo à Pesquisa do Estado de São Paulo (FAPESP).

[1] B. Grabmaier and R. Oberschmid, Phys. Status Solidi A **96**, 199 (1986).
[2] J. Frejlich and P. M. Garcia, Opt. Lasers Eng. **32**, 515 (1999).
[3] A. A. Kamshilin and M. P. Petrov, Opt. Commun. **53**, 23 (1985).
[4] S. Mallick and D. Rouède, Appl. Phys. B: Photophys. Laser Chem. **43**, 239 (1987).
[5] L. Mosquera, I. de Oliveira, J. Frejlich, A. Hernandes, S. Lanfredi, and J. Carvalho, J. Appl. Phys. **90**, 2635 (2001).
[6] V. Marinova, S. Lin, V. Sainov, M. Gospodinov, and K. Hsu, J. Opt. A, Pure Appl. Opt. **5**, S500 (2003).
[7] S. G. Odoulov, K. V. Shcherbin, and A. N. Shumeljuk, J. Opt. Soc. Am. B **11**, 1780 (1994).
[8] V. V. Prokofiev *et al.*, Cryst. Res. Technol. **30**, 171 (1995).
[9] J. F. Carvalho and A. C. Hernandes, Cryst. Res. Technol. **40**, 847 (2005).
[10] A. Lobato, S. Lanfredi, J. F. Carvalho, and A. Hernandes, Mater. Res. **3**, 92 (2000).
[11] H. Oheda, J. Appl. Phys. **52**, 6693 (1981).
[12] C. Longeaud and J. Kleider, Phys. Rev. B **45**, 11672 (1992).
[13] J. P. Kleider and C. Longeaud, in *Solid State Phenomena*, edited by H. Neber-Aeschbacher (Scitec, Zurich, 1995).
[14] C. Longeaud, J. Kleider, P. Kaminski, R. Koslowski, M. Pawlowski, and R. Cwirko, Semicond. Sci. Technol. **14**, 747 (1999).
[15] R. Montenegro, N. R. Inocente-Junior, and J. Frejlich, Rev. Sci. Instrum. **77**, 043905 (2006).
[16] C. Coya, C. Zaldo, V. Volkov, A. Egorysheva, K. Polgár, and A. Péter, J. Opt. Soc. Am. B **13**, 908 (1996).
[17] K. Buse, Appl. Phys. B: Lasers Opt. **64**, 273 (1997).
[18] P. V. dos Santos, J. F. Carvalho, and J. Frejlich, Opt. Mater. **29**, 642 (2007).

[19]R. Aldrich, S. Hou, and M. Harvill, J. Appl. Phys. **42**, 493 (1971).
[20]J. A. Baquedano, L. Contreras, E. Diéguez, and J. Cabrera, J. Appl. Phys. **66**, 5146 (1989).
[21]P. dos Santos, J. Carvalho, and J. Frejlich, Appl. Phys. B: Lasers Opt. **81**, 651 (2005).
[22]J. Frejlich and P. M. Garcia, Appl. Phys. A: Solids Surf. **55**, 49 (1992).
[23]A. Delboulbe, C. Fromont, J. Herriau, S. Mallick, and J. Huignard, Appl. Phys. Lett. **55**, 713 (1989).
[24]S. Riehemann, F. Rickermann, V. Volkov, A. Egorysheva, and G. von Bally, J. Nonlinear Opt. Phys. Mater. **6**, 235 (1997).
[25]A. Ennouri, M. Tapiero, J. Vola, J. Zielinger, J. Moisan, and J. Launay, J. Appl. Phys. **74**, 2180 (1993).